THE JOURNAL OF PHYSICAL CHEMISTRY A

 VOLUME 106, NUMBER 46, NOVEMBER 21, 2002

ARTICLES

Thermal Fluctuations of the Unusually Symmetric and Stable Superoxide Tetrahydrate Complex: An ab Initio Molecular Dynamics Study

I-Feng W. Kuo and Douglas J. Tobias*

Department of Chemistry, University of California, Irvine, California 92697-2025

Received: August 29, 2002

We report an ab initio molecular dynamics simulation study of a complex composed of the superoxide anion and four water molecules. We probe the symmetry and stability of the superoxide tetrahydrate anion cluster at a low temperature (25 K) where there are vibrational spectra and a higher temperature (111 K) where experimental data are not available. From the ab initio simulation trajectory, we found the superoxide tetrahydrate complex to be highly symmetric, exhibiting a collective breathing motion on the picosecond time scale at low temperature that subsequently disappears at higher temperatures. Furthermore, we establish that superoxide tetrahydrate is a highly stable species at the higher temperature with little or no distortion to its geometry. The vibrational spectrum calculated from our ab initio trajectory is in reasonable agreement with experimental spectra, and we were able to assign individual peaks in the spectra to specific modes in the superoxide tetrahydrate anion cluster.

Introduction

The superoxide radical anion (O_2^-) plays important roles in both atmospheric chemistry as well as in disrupting fundamental biological functions in cellular biology. In the atmosphere, the superoxide anion is known to be involved in regulating the overall oxidizing capacity of the troposphere as well as in key reactions that cause the destruction of ozone in the aqueous phase.[1] In the cell, superoxide is considered to be a reactive oxygen species that includes other molecular members such as singlet oxygen, hydroxyl radical, hydrogen peroxide, and nitric oxide.[2] Due to the unpaired electron, members of this group are highly reactive and cause adverse effects in cellular environments. Consequently, there are highly efficient evolutionary mechanisms that help to rapidly remove such radical species. The function of the protein superoxide dismutase is the rapid conversion of superoxide anion into hydroxyl radicals that can be further processed and removed.[2]

Due to the prevalence of water in both cellular and atmospheric environments, the structure and properties of superoxide ion and its aqueous solvation shell are of interest. Electron spin resonance (ESR) measurements on frozen solutions have shown that the hydration shell of the superoxide anion is relatively small, with only four protons being strongly coupled to the unpaired electrons.[3−5] Recent experiments using argon nanomatrixes with infrared spectroscopy,[6] which dramatically sharpens mid-IR bands, have also shed some light on the hydration of superoxide anion. With the sharpened resolution in the mid-IR range around OH vibrational frequencies, a structure was assigned for the superoxide tetrahydrate complex that matches the OH vibrations observed.[7,8] Further insight into the solvation of superoxide anion was obtained using photoelectron photofragment coincidence spectroscopy, which shows a significant change in the energetics for the solvation of the superoxide complex beyond four waters.[9] From all the experiments, the consensus is that the tetracoordinated superoxide complex is a relatively stable species when compared to one to three water complexes. Superoxide anion−water interactions have also been studied theoretically using ab initio calculations on small clusters

10.1021/jp026873s CCC: $22.00
Published on Web 10/22/2002

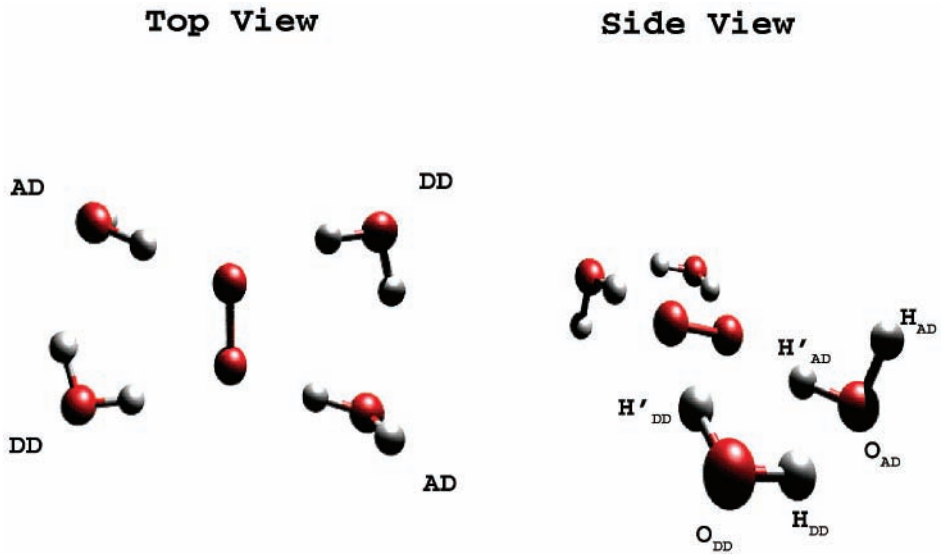

Figure 1. Structure and labeling of the superoxide tetrahydrate complex. The acceptor−donor (AD) and donor−donor (DD) waters are labeled according to the hydrogen bonds present. Individual atoms for the water molecules are labeled where the subscript signifies the type of water and the presence of the prime signifies the hydrogen closer to the superoxide anion. The atoms on the superoxide anion are simply referred to as "O". The structures presented are the optimized geometry from CPMD with the BLYP functional and a plane wave basis set expanded to an energy cutoff of 100 Ryd.

containing one to four waters[10,11] all the way to bulk using empirical force fields and molecular dynamics simulation.[12] For small complexes, $(O_2^-(H_2O)_n)$ ($n = 1-4$), early ab initio studies using unrestricted Hartree−Fock (UHF) and Moller−Plesset (MP) perturbation methods with minimal basis sets have shown that the differences in energy for different minimum energy geometries are small, and thus the potential energy surfaces are relatively flat.[10,11]

A highly symmetric structure for the superoxide tetrahydrate complex was hinted at by early ESR studies[4] and confirmed recently by assigning peaks in the IR spectra[7,8] on the basis of similarity to the spectra of $X^-(H_2O)_2$ halide−water clusters[13] (which have been probed theoretically for thermal effects[14] and anharmonicity[15] of the OH vibrational mode using a modified RWK2[16] water potential). In this paper we will provide additional insight into the symmetry and electronic structure as well as the thermal stability of the superoxide tetrahydrate complex obtained from ab initio molecular dynamics (MD) simulations carried out using the Kohn−Sham formulation of density functional theory[17−19] (DFT) with a plane wave basis set. Furthermore, we will show that DFT with the BLYP exchange-correlation functional provides results in good qualitative agreement with experimental vibrational spectra, and that the molecular dynamics simulations are useful for interpreting the spectra.

Computational Details

Geometry optimization was performed in the gas phase using the Kohn−Sham formulation of density functional theory (DFT) within the appropriate spin density approximation.[17−19] Two types of exchange and correlation functionals were used in optimizing the structure of superoxide tetrahydrate. One was a hybrid functional that incorporates Becke's 3-parameter exchange[20] with the Lee−Yang−Parr[21] correlation (B3LYP), as implemented in Gaussian98.[22] The basis sets chosen for the B3LYP calculations were augmented correlation consistent polarized valence double-ζ (aug-cc-pvdz) and triple-ζ (aug-cc-pvtz). Also included for completeness are the 6-311+G(2d,p) basis set used by Weber et al.[7,8] In addition, the Becke[23] exchange with the Lee−Yang−Parr[21] correlation (BLYP) functional was used in conjunction with the aug-cc-pvdz and aug-cc-pvtz basis sets as implemented in Gaussian98,[22] and a plane wave (PW) basis set as implemented in CPMD[24] with the Kohn−Sham orbitals expanded to an energy cutoff of 100 Rydberg. In the BLYP with plane wave basis set calculations, the valence electrons were treated explicitly and the valence−core interactions were described by norm-conserving pseudopotentials of the Troullier−Martins form.[25] For the plane wave geometry optimization, the superoxide tetrahydate complex (Figure 1) was optimized in a cubic periodic box with edge length 15.9 Å incorporating cluster boundary conditions.[26] The optimization was stopped when the root-mean-squared gradient was less than 10^{-4} for the nuclei.

All ab initio MD trajectories were generated using the CPMD[24] simulation package with the BLYP electronic structure methodology described above with a plane wave basis set expanded to 100 Rydberg. For the ab initio MD simulations, the system was placed in a cubic periodic box of 10.6 Å in conjunction with cluster boundary conditions[26] to reduce the computational expenditure after it was found that the reduced cell size has no effect on the minimum energy geometry. The equations of motion for the electrons and ions were integrated using the method of Car and Parrinello[27] with a fictitious electron mass of 800 au and a time step of 0.121 fs in the microcanonical (NVE) ensemble. For the superoxide tetrahydrate system, two trajectories were generated with average temperatures of 25 and 111 K. For both trajectories, a 5.5 ps production run was obtained after 0.5 ps equilibration time. The ab initio simulations required approximately 37 wallclock hours per picosecond of trajectory using 16 CPUs and 1435 MB of memory on an IBM SP2.

Due to the large ficticious electronic mass used to permit the large integration time step of 0.121 fs, a retardation of the nuclear motion occurs with the most pronounced effect on light nuclei such as hydrogen. As a result, MD spectra and vibrational frequencies reported here are scaled by 1.077 to give results in the domain where the fictitious electronic mass approaches zero and spectral frequencies approach their true frequency in the absence of the drag induced by the fictitious electronic mass. The scaling factor 1.077 was derived from a series of ab initio

TABLE 1: Vibrational Modes of Water Monomer[a]

cutoff/EMass	AS	SS	scaling
70 Ryd/harmonic	3635	3536	1.000
70 Ryd/200 au	3573	3471	1.017
70 Ryd/400 au	3508	3412	1.036
70 Ryd/600 au	3444	3349	1.055
70 Ryd/800 au	3379	3286	1.076
100 Ryd/harmonic	3788	3685	1.000
100 Ryd/200 au	3723	3622	1.017
100 Ryd/400 au	3655	3556	1.036
100 Ryd/800 au	3518	3422	1.077

[a] The asymmetric (AS) and symmetric (SS) frequencies of the water monomer as computed using harmonic approximation and ab initio MD simulation at 5 K.

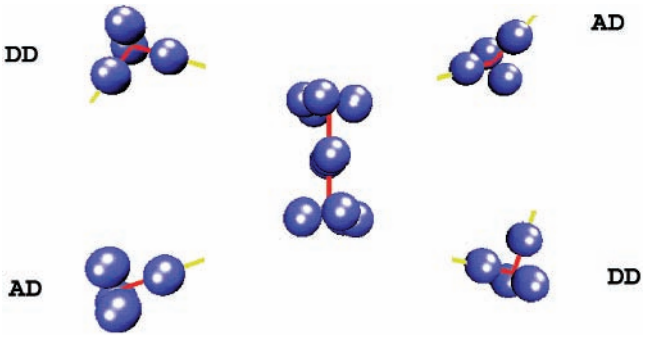

Figure 2. Maximally localized Wannier functions obtained from the transformation of the Kohn−Sham orbitals for the superoxide tetrahydrate complex. The blue spheres represent the Wannier function centers that were used in our dipole moment calculations, and the red and yellow lines represent the water OH bonds and the OO superoxide bond, respectively.

MD simulations of water monomer in a cubic box of 7.9 Å at 5 K. The simulations were run with a time step of 0.0242 fs and energy cutoff for the plane waves at 70 and 100 Ryd. The asymmetric and symmetric stretch frequencies were recorded (Table 1). The scaling factor was obtained as the ratio of the harmonic frequency of the asymmetric stretch to the frequencies obtained from MD simulations. It was found that the dynamic retardation on nuclear dynamics depends linearly on the electronic mass.[28] As a result, a scaling factor of 1.077 was applied to the spectral region of the OH vibrational frequencies.

We have employed a recent advancement in the analysis of electronic structure in a periodic system using a plane wave basis that involves the transformation of the Kohn−Sham orbitals into maximally localized Wannier functions,[29−32] as implemented in the CPMD program.[33] In this way, the total charge distribution in a system can be partitioned into individual molecular contributions (e.g., bonding pairs and lone pairs). The coordinates of the centers of these localized orbitals, the Wannier function centers (WFCs), can then be used in electrostatics calculations (e.g., calculation of dipole moments of individual molecules) (Figure 2).

Infrared (IR) spectra were computed using the following expression for the IR absorption coefficient $\alpha(\omega)$:

$$\alpha(\omega) = \frac{4\pi\omega \tanh\left(\frac{\beta\hbar\omega}{2}\right)}{3\hbar n(\omega)cV} \int_{-\infty}^{\infty} dt\, e^{-i\omega t} \langle M(t)\cdot M(0)\rangle$$

where V is the volume, $\beta = 1/k_B T$, T is the temperature, and c is the speed of light.[34] The total dipole moment of the system, $M(t)$ (ionic plus electronic), was computed in the CPMD[24] program using a Berry phase scheme,[34−36] and the results reported here were obtained from the autocorrelation function, $\langle M(t)\cdot M(0)\rangle$, of the dipole moment using the maximum entropy method[37] (MEM). From previous ab initio MD simulations of $Cl^-(H_2O)_n$ ($n = 1-4$, 6), we have found that the calculated infrared spectra agree reasonably well with experimental spectra and, therefore, that the simulations can provide valuable insights into the origin of particular spectral features.[28,38] For peak assignments, we computed vibrational spectra from autocorrelation functions of bond stretching coordinates using the filter diagonalization method[39] (FDM).

Results and Discussion

Optimized Geometry of Superoxide Tetrahydrate in the Gas Phase. Using methods described above, the optimized geometry was obtained by using both B3LYP and BLYP functionals and several basis sets. A comparison of the different optimized geometries obtained indicates that BLYP accurately describes the structure of superoxide tetrahydrate when compared to the more accurate as well as computationally intensive B3LYP functional (Table 2). In particular, the intramolecular geometrical parameters are quite similar with deviations within 0.01 Å for bond lengths and 1° for angles, with the exception of the superoxide anion bond length, which has a difference of 0.03 Å between the two functionals. For intermolecular geometric parameters, the deviations between the two functionals are greater but are still within acceptable limits. The deviation between the two minimized structures can be due to either the basis set used in conjunction with B3LYP (see below) or the BLYP functional itself. Normal modes of superoxide tetrahydrate were calculated for both B3LYP and BLYP minimum energy structures. (Table 3) A comparison of the mid-IR region where the OH stretching frequencies are available from experiment is shown. It can be seen that the harmonic frequencies of both B3LYP and BLYP are off by as much as ~100 cm^{-1} for some OH stretches, but the spacing between the normal-mode frequencies are very similar. The overall good agreement of BLYP harmonic OH stretching frequencies with experiment found here and in studies of other ion−water clusters is fortuitous. When anharmonicity and coupling between modes are taken into account, the accuracy of BLYP frequencies worsens considerably.[40,41] We will return to this issue below in our discussion of vibrational spectra computed from the MD simulations.

Basis Set Dependence. By using different basis sets, we were able to determine the effects varying basis sets have on the optimized geometric parameters for the superoxide tetrahydrate complex. Within the B3LYP exchange and correlation functional, the optimized geometries using aug-cc-pvdz and aug-cc-pvtz basis sets yield comparable results with bond lengths typically within 0.01 Å and angles within 1°. When the augmented correlation consistent basis sets were compared to the previously optimized structure using Pople's 6-311+G(2d,p) basis set,[7,8] the results were comparable with a few notable exceptions. With the Pople basis set, the intramolecular O−O distance for superoxide was overestimated by 0.03 Å, whereas the $O_{AD}-H_{AD}$ bond length was 0.05 Å longer than corresponding calculations using the aug-cc-pvdz and aug-cc-pvtz basis sets with the B3LYP functional. For intermolecular distances, the major difference between the basis sets is the $O-H'_{DD}$ distance, which is 0.04 Å longer with the Pople basis set compared to the aug-cc-pvtz basis set.

For the geometry optimization using the BLYP exchange and correlation functional, we were able to compare results obtained using a converged plane wave basis set to the augmented correlation consistent basis sets. As before, the geometric

TABLE 2: Optimized Geometries of Superoxide Tetrahydrate Anion

parameters[a]	B3LYP[b] 6-311+G(2d,p)	B3LYP[c] aug-cc-pvdz	B3LYP[c] aug-cc-pvtz	BLYP[c] aug-cc-pvdz	BLYP[c] aug-cc-pvtz	BLYP[c] PW
O−O[d]	1.363	1.330	1.330	1.361	1.362	1.368
$O-O_{AD}$	2.717	2.702	2.705	2.721	2.725	2.728
$O-O_{DD}$	2.908	2.857	2.859	2.882	2.887	2.963
$O-O_{DD}$	2.908	2.857	2.859	2.882	2.887	2.962
$O-O_{AD}$	2.717	2.702	2.705	2.722	2.725	2.736
$O-H'_{AD}$	1.705	1.703	1.709	1.707	1.713	1.726
$O-H'_{DD}$	1.940	1.894	1.900	1.907	1.916	2.002
$O-H'_{DD}$	1.940	1.894	1.900	1.906	1.916	1.993
$O-H'_{AD}$	1.705	1.703	1.709	1.706	1.713	1.732
$O_{AD}-H_{DD}$	2.108	2.121	2.129	2.142	2.148	2.038
$O_{AD}-H_{DD}$	2.109	2.121	2.129	2.142	2.147	2.030
$O-H'_{AD}-O_{AD}$	175.19	176.33	176.31	177.10	177.17	173.06
$O-H'_{AD}-O_{AD}$	175.19	176.41	176.31	177.27	177.17	174.72
$O-H'_{DD}-O_{DD}$	164.82	166.03	165.76	166.36	165.96	168.04
$O-H'_{DD}-O_{DD}$	164.82	166.03	165.76	166.37	165.96	164.96
$O-O-H'_{AD}$	110.65	111.26	111.64	110.90	111.19	111.08
$O-O-H'_{AD}$	110.64	111.27	111.64	110.90	111.18	106.83
$O-O-H'_{DD}$	109.14	108.77	108.52	108.83	108.58	103.61
$O-O-H'_{DD}$	109.15	108.77	108.52	108.81	108.57	109.38
$O_{AD}-H_{AD}^{\ddagger}$	0.972	0.964	0.961	0.974	0.971	0.968
$O_{AD}-H'_{AD}{}^{\ddagger}$	1.014	1.001	0.998	1.015	1.012	1.007
$O_{DD}-H_{DD}^{\ddagger}$	0.981	0.971	0.968	0.982	0.979	0.976
$O_{DD}-H'_{DD}{}^{\ddagger}$	0.991	0.982	0.979	0.994	0.990	0.984
$O_{DD}-H_{DD}^{\ddagger}$	0.981	0.971	0.968	0.982	0.979	0.975
$O_{DD}-H'_{DD}{}^{\ddagger}$	0.991	0.982	0.979	0.994	0.990	0.983
$O_{AD}-H_{AD}^{\ddagger}$	1.014	0.964	0.961	0.974	0.971	1.006
$O_{AD}-H'_{AD}{}^{\ddagger}$	0.972	1.001	0.998	1.015	1.012	0.967
$H_{AD}-O_{AD}-H'_{AD}{}^{\ddagger}$	103.51	103.54	103.96	103.13	103.52	102.55
$H_{DD}-O_{DD}-H'_{DD}{}^{\ddagger}$	100.62	111.96	101.38	100.35	100.77	101.37
$H_{AD}-O_{AD}-H'_{AD}{}^{\ddagger}$	103.52	103.55	103.96	103.14	103.52	103.81
$H_{DD}-O_{DD}-H'_{DD}{}^{\ddagger}$	100.62	100.95	101.38	100.35	100.77	100.38

[a] All units are in ångstroms for bond lengths and degrees for angles. "AD" signifies acceptor−donor water and "DD" signifies donor−donor water in the superoxide tetrahydrate structure. (See Figure 1.) [b] Weber et al.[7] [c] This work. [d] Intramolecular distances or angles.

TABLE 3: Vibrational Frequencies of OH Bonds[a]

OH stretch[b]	B3LYP[c] 6-311+G(2d,p)	B3LYP[d] aug-cc-pvtz	BLYP[d] aug-cc-pvtz	BLYP[d] PW	BLYP[d] (MD 25 K)	exp[c]
F-OH	3870	3855	3711	3763	3438	3690
IW-OH	3736	3731	3573	3621	3391	3615
DD-IHB	3572, 3548	3530, 3504	3372, 3345	3487	∼3115−3223	3300
AD-IHB	3180, 3130	3173, 3126	2987, 2939	3083	∼2900	2950

[a] Vibrational frequencies where F-OH, IW-OH, DD-IHB, and AD-IHB are the bond vibration for $O_{AD}-H_{AD}$, $O_{DD}-H_{DD}$, $O_{DD}-H'_{DD}$, and $O_{AD}-H'_{AD}$ respectively. [b] All frequencies are in wavenumbers (cm^{-1}). [c] Weber et al.[7] [d] This work.

parameters computed with the aug-cc-pvdz and aug-cc-pvtz basis sets were comparable, with typical length deviations less than 0.01 Å and angles less than 1°. For the plane wave basis set geometry optimization, most of the intermolecular distances were longer and the intramolecular distances were shorter compared to the aug-cc-pvtz basis set. The largest differences were for geometric parameters related to the double donor water, where the $O-H'_{DD}$ and $O-O_{DD}$ distances were 0.09 Å longer in the plane wave calculation compared to the aug-cc-pvtz calculation. Furthermore, the predicted distance between $O_{AD}-H_{DD}$ is 0.11 Å shorter when using the plane wave basis set.

Average Geometry of Superoxide Tetrahydrate from ab Initio MD Simulations. From our low temperature ab initio MD trajectory at 25 K, we noticed that the thermal fluctuation of the structure is relatively low, with little or no deviation from the optimized structure (Figure 3) with two notable exceptions. First, the $O-H'_{AD}-O_{AD}-H_{AD}$ dihedral angles exhibited large fluctuations (with standard deviations of 46° and 40°), as can be seen in Figure 4 even at 25 K. The large standard deviation is due to the softness of the $O-H'_{AD}-O_{AD}-H_{AD}$ mode. The average dihedral angles ($O-H'_{AD}-O_{AD}-H_{AD}$) observed in the MD simulation were 215° and 147°, which are comparable to the 216° and 144° obtained from the geometry optimization using B3LYP with aug-cc-pvtz basis set. The second exception involves the intramolecular bond angle involving the two acceptor−donor (AD) waters, which increased slightly by approximately 2°, a deviation that exceeds the standard deviation of around 1.3° (Table 4). With respect to intermolecular geometric parameters involving acceptor−donor (AD) waters, the average structure from our 25 K trajectory shows only small changes that are within the standard deviations and thus are effectively similar to the minimized structure. Although acceptor−donor (AD) intermolecular distances are relatively unchanged, in our low-temperature simulation we noticed both lengthening and shortening of intermolecular distance parameters involving donor−donor (DD) water molecules. In particular both $O-O_{DD}$ distances decreased by ∼0.09 Å. Likewise, both hydrogen bond $O-H_{DD}$ distances decreased about ∼0.1 Å along with a ∼0.19 Å increase in the two intermolecular hydrogen bond distances $O_{AD}-H_{DD}$.

For the high temperature ab initio MD simulation at 111 K, the same pattern of geometric deformation is seen as in the low-temperature trajectory, where the intramolecular bond lengths and angles remain close to the optimized geometry. The intermolecular distances involving the acceptor−donor waters remain relatively unchanged whereas the intermolecular distances involving donor−donor waters change more dramatically, as expected from the greater thermal sampling at higher

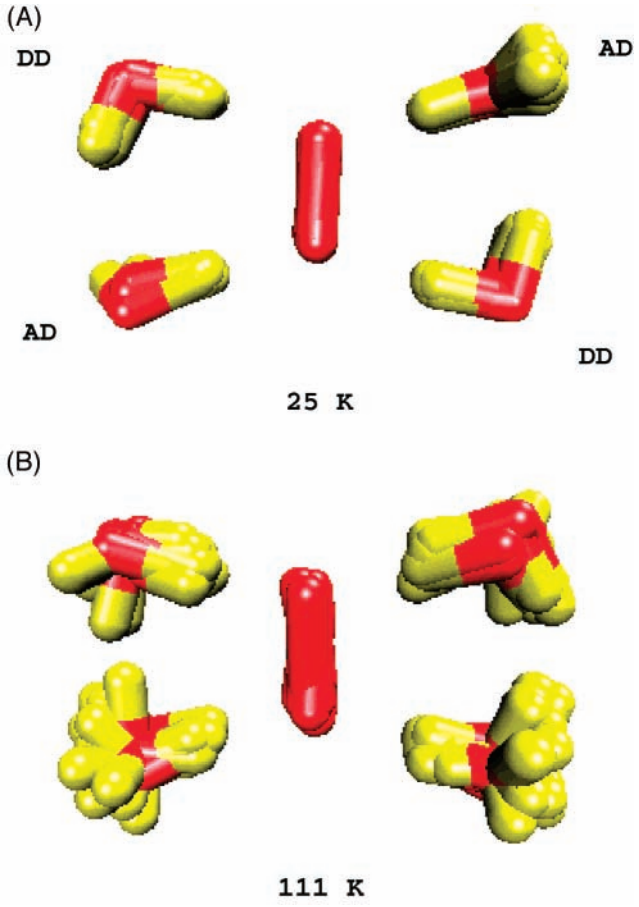

Figure 3. Overlay of superoxide tetrahydrate structures at (A) 25 K and (B) 111 K over 5.5 ps at 0.37 ps intervals.

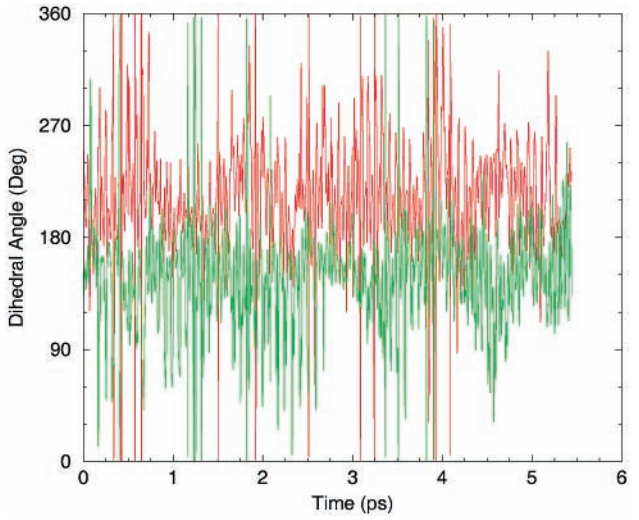

Figure 4. Time histories of the two dihedral angles ($O-H'_{AD}-O_{AD}-H_{AD}$) from the ab initio MD simulation at 25 K. The averages are 215 ± 46° and 147 ± 40° (trans = 180°).

temperature. In particular, the two intermolecular water hydrogen bonds as measured by the $O_{AD}-H_{DD}$ distances increased by ~0.9 Å, which is a significant deviation from the optimized geometry. In addition, the increase in temperature from 25 to 111 K also allowed greater sampling and almost free rotation for the $O-H'_{AD}-O_{AD}-H_{AD}$ dihedral angle. Although the superoxide anion is a highly reactive species, in our comparison of the high and low temperature average structures of superoxide tetrahydrate to its minimum energy geometry, we found that its highly symmetric, nearly planar complex with four water molecules is quite stable and robust (Figure 3).

TABLE 4: Superoxide Tetrahydate Anion Geometries

parameters[a]	optimized geometry[b]	MD 25 K[c]	MD 111 K[d]
$O-O^e$	1.368	1.367 ± 0.019	1.366 ± 0.024
$O-O_{AD}$	2.728	2.724 ± 0.037	2.857 ± 0.121
$O-O_{DD}$	2.963	2.870 ± 0.070	2.821 ± 0.124
$O-O_{DD}$	2.962	2.865 ± 0.063	2.827 ± 0.136
$O-O_{AD}$	2.736	2.721 ± 0.033	2.859 ± 0.151
$O-H'_{AD}$	1.726	1.722 ± 0.039	1.879 ± 0.138
$O-H'_{DD}$	2.002	1.897 ± 0.079	1.832 ± 0.142
$O-H'_{DD}$	1.993	1.892 ± 0.072	1.843 ± 0.157
$O-H'_{AD}$	1.732	1.719 ± 0.034	1.876 ± 0.180
$O_{AD}-H_{DD}$	2.038	2.216 ± 0.146	3.016 ± 0.560
$O_{AD}-H_{DD}$	2.030	2.219 ± 0.149	2.900 ± 0.555
$O-H'_{AD}-O_{AD}$	173.06	175.42 ± 2.07	166.16 ± 7.53
$O-H'_{AD}-O_{AD}$	174.72	175.26 ± 2.18	167.89 ± 7.73
$O-H'_{DD}-O_{DD}$	168.04	168.60 ± 3.96	167.16 ± 7.25
$O-H'_{DD}-O_{DD}$	164.96	168.53 ± 4.04	168.92 ± 6.94
$O-O-H'_{AD}$	111.08	110.56 ± 2.29	110.40 ± 7.09
$O-O-H'_{AD}$	106.83	110.52 ± 2.42	109.71 ± 5.70
$O-O-H'_{DD}$	103.61	108.75 ± 2.19	109.65 ± 6.20
$O-O-H'_{DD}$	109.38	108.70 ± 2.53	109.72 ± 5.93
$O_{AD}-H_{AD}^e$	0.968	0.966 ± 0.002	0.977 ± 0.014
$O_{AD}-H'_{AD}{}^e$	1.007	1.005 ± 0.004	1.003 ± 0.012
$O_{DD}-H_{DD}^e$	0.976	0.973 ± 0.003	0.976 ± 0.006
$O_{DD}-H'_{DD}{}^e$	0.984	0.988 ± 0.004	1.006 ± 0.013
$O_{DD}-H_{DD}^e$	0.975	0.973 ± 0.005	0.979 ± 0.008
$O_{DD}-H'_{DD}{}^e$	0.983	0.988 ± 0.004	1.006 ± 0.012
$O_{AD}-H_{AD}^e$	1.006	1.005 ± 0.004	1.004 ± 0.013
$O_{AD}-H'_{AD}{}^e$	0.967	0.966 ± 0.002	0.977 ± 0.007
$H_{AD}-O_{AD}-H'_{AD}{}^e$	102.55	105.86 ± 1.33	102.98 ± 4.27
$H_{DD}-O_{DD}-H'_{DD}{}^e$	101.37	101.84 ± 1.09	103.34 ± 2.83
$H_{AD}-O_{AD}-H'_{AD}{}^e$	103.81	101.86 ± 1.09	103.46 ± 3.19
$H_{DD}-O_{DD}-H'_{DD}{}^e$	100.38	105.95 ± 1.36	102.84 ± 2.93

[a] All units are in ångstroms for bond lengths and degrees for angles. "AD" signifies acceptor−donor water and "DD" signifies donor−donor water in the superoxide tetrahydrate structure. (See Figure 1.) [b] Optimized geometry from CPMD with the BLYP functional and a plane wave basis set expanded to an energy cutoff of 100 rydberg. [c] Average geometry and standard deviation obtained from ab initio MD simulation at 25 K. [d] Average geometry and standard deviation obtained from ab initio MD simulation at 111 K. [e] Intramolecular distances or angles.

Electronic Structure of Water. In the ab initio MD simulation the electronic structure of the water molecules fluctuates naturally in response to changes in the structure of the superoxide tetrahydrate complex. These fluctuations are reflected in the changes of the dipole moments of the individual water molecules, which may be computed from the position of the ions and WFCs positions, assuming that the electronic charge is concentrated in point charges located on the WFCs. As can be seen in Figure 5, at 25 K the dipole distributions of the four waters can be partitioned into two distinct types that we previously labeled as acceptor−donor (AD) and donor−donor (DD) waters in the structures (Figure 1). Furthermore, throughout the simulation, there was no exchange between the two types of waters. The calculated average dipole moment is 2.46 ± 0.06 D for the two acceptor−donor (AD) and 2.58 ± 0.04 D for the two donor−donor (DD) waters. These values are significantly larger than the 1.87 and 2.15 D computed for the water monomer or dimer, respectively, in the gas phase.[42] The larger average dipole in the donor−donor (DD) water is due to the increased perturbation of the electronic structure resulting from the extra hydrogen bond.

Whereas the average geometry at 111 K still allows the distinct identification and categorization of the four waters as

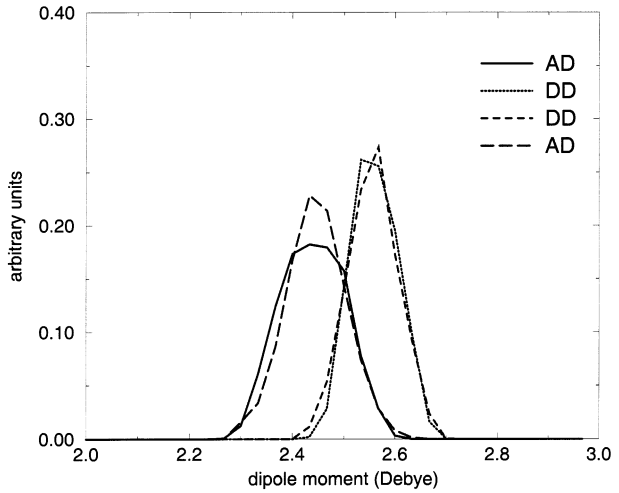

Figure 5. Histogram of water dipole moments at 25 K. The four waters are assigned as acceptor−donor (AD) or donor−donor (DD) according to the optimized geometry (see Figure 1).

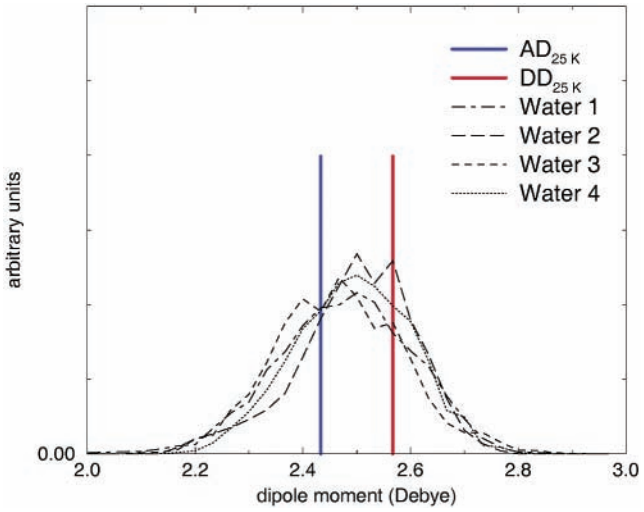

Figure 6. Histogram of water dipole moments of four individual waters at 111 K along with the average dipole moments (indicated by vertical lines) of AD and DD waters from the 25 K trajectory.

either acceptor−donor (AD) or donor−donor (DD), a look at the water dipoles shows that the distinguishability between the two types of water starts to fade. For the four individual waters, the average dipole moments are 2.49 ± 0.12, 2.51 ± 0.11, 2.52 ± 0.11, and 2.48 ± 0.12 D. The first two values correspond to the waters that were previously identified as acceptor−donor (AD) and the latter two to donor−donor (DD). Figure 6 shows that the dipole moment distributions for the four waters are effectively indistinguishable at 111 K, in contrast to the low temperature distribution. Because the dipole of each water molecule is highly sensitive to the environment, it can be concluded that as the temperature increases, the waters will slowly become indistinguishable and will effectively become interchangeable when thermal fluctuations dominate.

Infrared and Vibrational Spectra. The infrared spectrum for superoxide tetrahydrate anion calculated from the total dipole moment autocorrelation function at 25 K is shown in Figure 7A. In the experimental spectrum,[7] the peaks in the mid-IR region were assigned on the basis of its similarity to spectra of $X^-(H_2O)_2$ (X = halogens) clusters. We were able to assign the peaks through the use of spectral analysis of velocity autocorrelation functions for bond stretching coordinates. It was found that the $O_{AD}-H_{AD}$ bond that is hydrogen bonded to

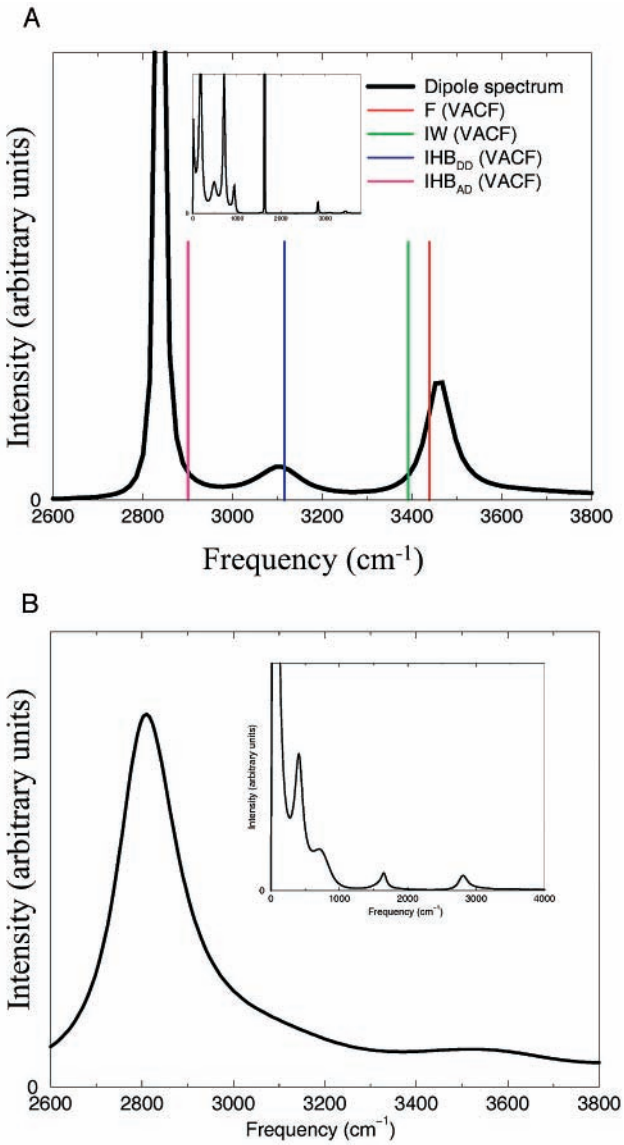

Figure 7. Infrared spectrum for superoxide tetrahydrate computed from the total dipole moment autocorrelation function. (A) 25 K. Frequencies of peaks in the spectra of the OH velocity autocorrelation functions are indicated by vertical lines. ($F = O_{AD}-H_{AD}$, $IW = O_{DD}-H_{DD}$, $IHB_{DD} = O_{DD}-H'_{DD}$, and $IHB_{AD} = O_{AD}-H'_{AD}$). (B) 111 K.

superoxide has a vibrational frequency of 2900 cm^{-1}. The $O_{AD}-H_{AD}$ bond with no hydrogen bond has a vibrational frequency of 3438 cm^{-1}. The $O_{DD}-H_{DD}$ bond that hydrogen bonds to superoxide has a vibrational frequency of 3115 cm^{-1}, and the $O_{DD}-H_{DD}$ bond that forms an intermolecular hydrogen bond between the waters has a vibrational frequency of 3391 cm^{-1}. Although the frequencies obtained from our spectra are not in quantitative agreement with experimental frequencies measured in argon clusters (Table 3), the assignment of the vibrational frequencies (see below) is in agreement. One possible reason for the discrepancies in the frequencies is deficiencies in the BLYP functional.[40,41]

From our simulation results, we found that the highest vibrational frequency is the $O_{AD}-H'_{AD}$ stretch followed by the $O_{DD}-H_{DD}$, $O_{DD}-H'_{DD}$, and $O_{AD}-H'_{AD}$ stretches. $O_{AD}-H'_{AD}$ can be referred to as the free OH (F-OH) due to its lack of hydrogen bonds, and $O_{DD}-H_{DD}$ can be refer to as the interwater OH (IW-OH) for its similarity to hydrogen bonding in bulk water. $O_{AD}-H'_{AD}$ and $O_{AD}-H'_{AD}$ have ionic hydrogen bonding environments; thus they are referred to as DD-IHB and AD-

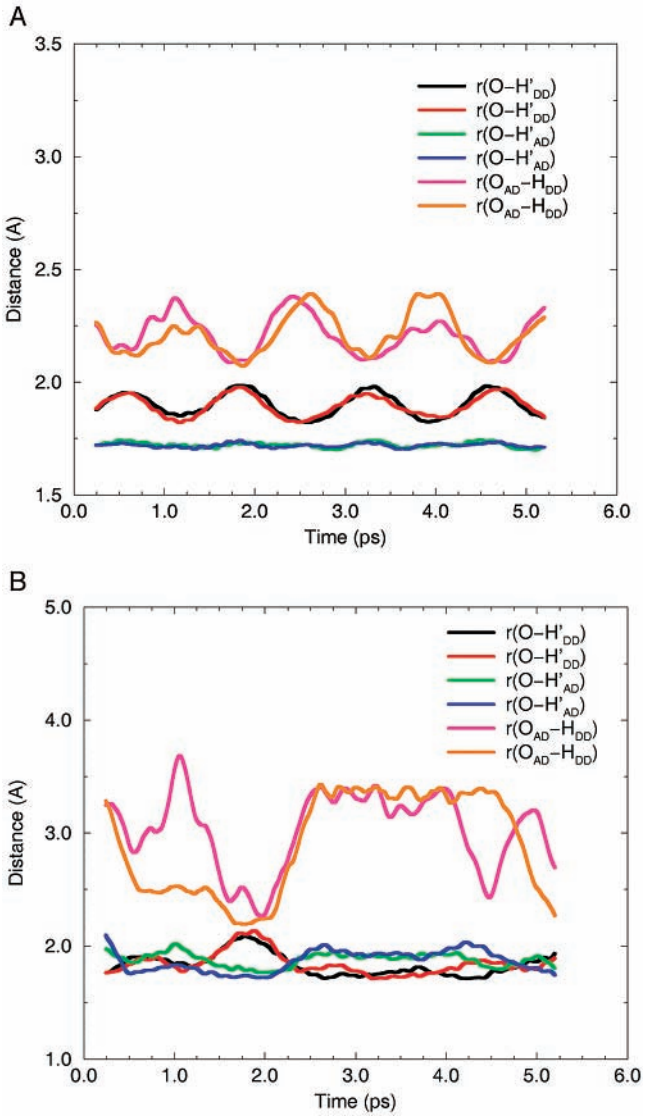

Figure 8. Intermolecular hydrogen bond distances for all hydrogen bonds in the superoxide tetrahydrate complex. The hydrogen bonds can be classified into three groups: $O-H'_{AD}$, $O-H'_{DD}$, and $O_{AD}-H_{DD}$. (A) At 25 K, the three types of hydrogen bonds are clearly distinguishable from each other. (B) At 111 K, $O-H'_{AD}$ and $O-H'_{DD}$ have become identical whereas the $O_{AD}-H_{DD}$ hydrogen bond distance has increased dramatically due to the greater thermal motion of the system.

IHB for the donor−donor or acceptor−donor waters, respectively. Therefore, from our simulation results, we found that the highest vibrational frequency is due to the F-OH, followed by IW-OH, DD-IHB, and AD-IHB (Figure 7A), which are the same conclusions reached by Weber et al.[7,8]

At 111 K, the simulated infrared spectrum for superoxide tetrahydrate anion (Figure 7B) shows thermal effects in the disruption of the hydrogen bonds analogous to those observed in simulations of the $Cl^-(H_2O)_2$ cluster by Dorsett et al.[14] From experimental spectra without argon cooling, and hence with higher internal energies,[8] a similar disruption of the hydrogen bonding network was observed when compared to spectra of superoxide tetrahydrate clusters that were cooled into their minimum energy configuration. In particular, the ionic hydrogen bonds, identified at 25 K as $O_{AD}-H'_{AD}$ and $O_{DD}-H'_{DD}$, have collapsed into one broad band, whereas the bands previously identified as F-OH and IW-OH remain the same.

Collective Dynamics. In our low temperature ab initio trajectory, it is evident from fluctuations in the hydrogen bond lengths that there is a long time scale collective fluctuation of the structure of the cluster. This can most clearly be seen when a coarse grained average is employed to remove faster oscillations, as in Figure 8A. From the figure, it can be noted that the $O-H'_{AD}$ hydrogen bond length oscillates with a period of approximately 1.25 ps. Interestingly, in the same figure, the $O_{AD}-H_{DD}$ hydrogen bond length oscillates at roughly the same frequency. A period of 1.25 ps corresponds to a vibrational frequency of $\sim$25 cm^{-1}. The two hydrogen bond lengths are effectively oscillating at the same frequency but are out of phase with each other. By performing a similar analysis on other structural features, we found that this behavior is reflected in all the other intermolecular geometric parameters in our 25 K ab initio trajectory. A corresponding analysis of the ab initio trajectory at 111 K (Figure 8B**)** reveals that there are no long time scale collective oscillations at the higher temperature.

Conclusions

We have used ab initio MD simulations to study the structure and dynamics of the superoxide tetrahydrate complex ($O_2^-(H_2O)_4$) at 25 and 111 K. We found that the highly symmetric minimum energy structure of superoxide tetrahydrate was very stable in the sense that the average structure did not deviate significantly from the minimized structure at both 25 and 111 K. Analysis of the dynamics revealed that at 25 K the superoxide tetrahydrate anion exhibits a symmetric collective breathing motion on the picosecond time scale ($\sim$25 cm^{-1}) that expands and contracts the approximately rectangular cluster along its diagonals. In contrast, at 111 K the hydrogen bond coordinates exhibited predominantly random thermal motions and the collective mode identified at lower temperature was not observed. Furthermore, from our ab initio trajectories, we were able to generate an IR absorption spectrum of superoxide tetrahydrate and assign the highest frequency peaks to specific OH vibrations. Although our calculated frequencies are off compared to experimental results, they are shifted systematically and thus we can still use the simulations to assign peaks unambiguously. From our analysis, we conclude that the peak assignments made by Weber et al. based on an analogy to halide water clusters are in agreement with our ab initio MD results.

Acknowledgment. We thank the Maui High Performance Computing Center (MHPCC) for their generous allocation of computer time, and Vladimir Mandelshtam and Jianhan Chen for providing FDM codes for vibrational analysis.

References and Notes

(1) Wayne, R. P. *Chemistry of atmospheres*: *an introduction to the chemistry of the atmospheres of earth, the planets, and their satellites*, 2nd ed.; Clarendon Press: Oxford University Press: Oxford, England, 1991.
(2) Voet, D.; Voet, J. G. *Biochemistry*; Wiley: New York, 1990.
(3) Symons, M. C. R.; Eastland, G. W.; Denny, L. R. *J. Chem. Soc., Faraday Trans.* **1980**, *1*, 1868.
(4) Narayana, P. A.; Suryanarayana, D.; Kevan, L. *J. Am. Chem. Soc.* **1982**, *104*, 3552.
(5) Bagchi, R. N.; Bond, A. M.; Scholz, F.; Stosser, R. *J. Am. Chem. Soc.* **1989**, *111*, 8270−8271.
(6) Johnson, M. A.; Lineberger, W. C. *Techniques for the Study of Ion−Molecule Reactions*, Farrar, J. M., Saunders, W. H., Ed.; Wiley-Interscience: New York, 1988; p 591.
(7) Weber, J. M.; Kelley, J. A.; Nielsen, S. B.; Ayotte, P.; Johnson, M. A. *Science* **2000**, *287*, 2461−2463.
(8) Weber, J. M.; Kelley, J. A.; Robertson, W. H.; Johnson, M. A. *J. Chem. Phys.* **2001**, *114*, 2698−2706.
(9) Luong, A. K.; Clements, T. G.; Resat, M. S.; Continetti, R. E. *J. Chem. Phys.* **2001**, *114*, 3449−3455.
(10) Curtiss, L. A.; Melendres, C. A.; Reed, A. E.; Weinhold, F. *J. Comput. Chem.* **1986**, *7*, 294−305.
(11) Ohta, K.; Morokuma, K. *J. Phys. Chem.* **1987**, *91*, 401.

(12) Shen, J.; Wong, C. F.; McCammon, J. A. *J. Comput. Chem.* **1990**, *11*, 1003−1008.
(13) Ayotte, P.; Nielsen, S. B.; Weddle, G. H.; Johnson, M. A.; Xantheas, S. S. *J. Phys. Chem. A* **1999**, *103*, 10665−10669.
(14) Dorsett, H. E.; Watts, R. O.; Xantheas, S. S. *J. Phys. Chem. A* **1999**, *103*, 3351−3355.
(15) Schenter, G. K.; Garrett, B. C.; Voth, G. A. *J. Chem. Phys.* **2000**, *113*, 5171−5178.
(16) Reimers, J. R.; Watts, R. O.; Klein, M. L. *Chem. Phys.* **1982**, *64*, 95.
(17) Hohenberg, P.; Kohn, W. *Phys. Rev.* **1964**, *136*, B86.
(18) Kohn, W.; Sham, L. J. *Phys. Rev.* **1965**, *140*, A1133.
(19) Kohn, W.; Becke, A. D.; Parr, R. G. *J. Phys. Chem.* **1996**, *100*, 12974−12980.
(20) Becke, A. D. *J. Chem. Phys.* **1993**, *98*, 5648−5652.
(21) Lee, C.; Yang, W.; Parr, R. G. *Phys. Rev. B* **1988**, *37*, 785−789.
(22) Frisch, M. J.; Trucks, G. W.; Schlegel, H. B.; Scuseria, G. E.; Robb, M. A.; Cheeseman, J. R.; Zakrzewski, V. G.; Montgomery, J. A., Jr.; Stratmann, R. E.; Burant, J. C.; Dapprich, S.; Millam, J. M.; Daniels, A. D.; Kudin, K. N.; Strain, M. C.; Farkas, O.; Tomasi, J.; Barone, V.; Cossi, M.; Cammi, R.; Mennucci, B.; Pomelli, C.; Adamo, C.; Clifford, S.; Ochterski, J.; Petersson, G. A.; Ayala, P. Y.; Cui, Q.; Morokuma, K.; Malick, D. K.; Rabuck, A. D.; Raghavachari, K.; Foresman, J. B.; Cioslowski, J.; Ortiz, J. V.; Stefanov, B. B.; Liu, G.; Liashenko, A.; Piskorz, P.; Komaromi, I.; Gomperts, R.; Martin, R. L.; Fox, D. J.; Keith, T.; Al-Laham, M. A.; Peng, C. Y.; Nanayakkara, A.; Gonzalez, C.; Challacombe, M.; Gill, P. M. W.; Johnson, B. G.; Chen, W.; Wong, M. W.; Andres, J. L.; Head-Gordon, M.; Replogle, E. S.; Pople, J. A. *Gaussian 98*, revision A.6; Gaussian, Inc.: Pittsburgh, PA, 1998.
(23) Becke, A. D. *Phys. Rev. A* **1988**, *38*, 3098−3100.
(24) CPMD.; Hutter, J.; Alavi, A.; Deutsch, T.; Bernasconi, M.; Goedecker, S.; Marx, D.; Tuckerman, M.; Parrinello, M. MPI fur Festkorperforschung and IBM Zurich Research Laboratory, 3.3a ed., 1995−1999.
(25) Troullier, N.; Martins, J. L. *Phys. Rev. B* **1991**, *43*, 1993−2006.
(26) Martyna, G. J.; Tuckerman, M. E. *J. Chem. Phys.* **1999**, *110*, 2810−2821.
(27) Car, R.; Parrinello, M. *Phys. Rev. Lett.* **1985**, *55*, 2471−2474.
(28) Tobias, D. J.; Jungwirth, P.; Parrinello, M. *J. Chem. Phys.* **2001**, *114*, 7036−7044.
(29) Silvestrelli, P. L.; Marzari, N.; Vanderbilt, D.; Parrinello, M. *Solid State Commun.* **1998**, *107*, 7−11.
(30) Marzari, N.; Vanderbilt, D. *Phys. Rev. B* **1997**, *56*, 12847−12865.
(31) Boys, S. F. *Quantum theory of atoms, molecules, and the solid state; a tribute to John C. Slater*; Academic Press: New York, 1966; p 253.
(32) Vanderbilt, D.; King-Smith, R. D. *Phys. Rev. B* **1993**, *48*, 4442−4455.
(33) Berghold, G.; Mundy, C. J.; Romero, A. H.; Hutter, J.; Parrinello, M. *Phys. Rev. B* **2000**, *61*, 10040−10048.
(34) Silvestrelli, P. L.; Bernasconi, M.; Parrinello, M. *Chem. Phys. Lett.* **1997**, *277*, 478−482.
(35) Kingsmith, R. D.; Vanderbilt, D. *Phys. Rev. B* **1993**, *47*, 1651−1654.
(36) Resta, R. *Rev. Mod. Phys.* **1994**, *66*, 899−915.
(37) Press, W. H.; Numerical Recipes Software *Numerical recipes in C*, 2nd Version 2.02. ed.; Cambridge University Press: New York, 1992.
(38) Kuo, I. F.; Nguyen, Q. H.; Caballero, J.; Tobias, D. J. Manuscript in preperation.
(39) Mandelshtam, V. A. *Prog. Nucl. Magn. Reson. SP* **2001**, *38*, 159−196.
(40) Wright, N. J.; Gerber, R. B.; Tozer, D. J. *Chem. Phys. Lett.* **2000**, *324*, 206−212.
(41) Wright, N. J.; Gerber, R. B. *J. Chem. Phys.* **2000**, *112*, 2598−2604.
(42) Silvestrelli, P. L.; Parrinello, M. *Phys. Rev. Lett.* **1999**, *82*, 3308−3311.